Sensors & Actuators: B. Chemical 409 (2024) 135583

Contents lists available at ScienceDirect

Sensors and Actuators: B. Chemical

journal homepage: www.elsevier.com/locate/snb

Droplet microfluidic platform for extracellular vesicle isolation based on magnetic bead handling

Alessio Meggiolaro [a], Valentina Moccia [b], Alessandro Sammarco [c,d], Paola Brun [e], Carlotta Caterina Damanti [f,g], Beatrice Crestani [a], Lara Mussolin [f,g], Matteo Pierno [a], Giampaolo Mistura [a], Valentina Zappulli [b], Davide Ferraro [a,*]

[a] Department of Physics and Astronomy, University of Padova, Via Marzolo 8, Padova 35131, Italy
[b] Department of Comparative Biomedicine and Food Science, University of Padova, Viale dell'Università 16, Legnaro 35020, Italy
[c] Department of Neurology, Massachusetts General Hospital, 149 13th Street, Charlestown, MA 02129, USA
[d] Department of Urology, Houston Methodist Research Institute, 6670 Bertner Avenue, Houston, TX 77030, USA
[e] Department of Molecular Medicine, University of Padova, Via Gabelli 63, Padova 35121, Italy
[f] Department of Women and Child Health, University of Padova, Via Giustiniani 3, Padova 35128, Italy
[g] Istituto di Ricerca Pediatrica Città della Speranza, Corso Stati Uniti 4, Padova 35127, Italy

ARTICLE INFO

Keywords:
Microfluidics
Extracellular vesicle
Isolation
Magnetic bead

ABSTRACT

Extracellular vesicles (EVs) are rapidly gaining in popularity as biomarkers of various diseases, acting as cargoes of valuable information from the cell of origin. Despite their important value, their current use in clinical practice is still limited. One of the most limiting factors is their isolation. In fact, conventional approaches are characterized by low purity and throughput, or poor reproducibility. Here, we present a droplet microfluidic platform specifically developed for EV isolation by affinity capture with magnetic beads. This platform is capable of processing large sample volumes (2 mL) in a relatively short time (4.5 hours), with considerable automation. In detail, EVs and magnetic beads are co-encapsulated within the same droplet, which acts promoting their mixing due to the spontaneous recirculation; this continuous agitation prevents any loss usually caused by bead sedimentation and promotes the EV capturing. Our droplet microfluidic protocol is compared to a commercially available method, showing a shorter required incubation time (about 2.5 times) and a higher capture efficiency (2.5-folds). The microfluidic approach is therefore positively evaluated in terms of protein content, EV quantification and microRNA cargo analysis.

1. Introduction

Extracellular vesicles (EVs) are double-layered phospholipid vesicles with a nanometric size that are usually classified as small EVs (30–200 nm) or medium-large EVs (200–1000 nm) [1]. EVs, secreted by almost all cells, circulate in body fluids and transport lipids, proteins, and nucleic acids specific to the parental cells [2]. Originally considered cell waste, EVs are now well known as cargo-ships that carry, either inside or on their surfaces, useful genetic information and play an important role in cell-to-cell communication [3]. Among the possible cargoes, the preservation of microRNAs is particularly relevant, as these small noncoding RNAs, considered relevant biomarkers for the diagnosis of various diseases, are very prone to degradation [4].

Despite their extraordinary value, the use of EVs in clinical practice is currently still limited due to the great difficulties related to their isolation. In fact, conventional approaches based on the physical properties of EVs (size and density), such as ultracentrifugation (UC), size-exclusion chromatography (SEC), and density-gradient separation (DGS), suffer from low purity, poor reproducibility, or limited yields [5]. Importantly, reproducibility issues prevent the comparison with results obtained in different laboratories [6]. More recently, chemical affinity has been employed for the isolation of EVs by exploiting specific proteins present on their membranes, such as tetraspanins (e.g., CD63, CD81, CD9, etc.) [7]. To this end, open surfaces or micrometric beads can be coated with specific antibodies to target specific markers present on the vesicle membrane [8–10]. Although affinity capture approaches have already shown a higher purification rate than UC and DGS, they are less widely applied for isolation due to the long duration of the protocol,

* Corresponding author.
E-mail address: davide.ferraro@unipd.it (D. Ferraro).

https://doi.org/10.1016/j.snb.2024.135583
Received 7 November 2023; Received in revised form 30 January 2024; Accepted 1 March 2024
Available online 5 March 2024

which is still operator dependent [11]. Microfluidics has been employed over the past decade to overcome these limitations [12,13]. The first microfluidic devices, based on microchannels coated with specific antibodies devoted to the capture of EVs, showed promising results [14]. To increase the surface-to-volume ratio and improve the capture rate, functionalized patterns or nanoparticles were integrated within the microfluidic channel [15,16]. However, these systems suffer from clogging problems and complex microfabrication. In addition, being based on filtering, they are typically disposable. A promising different strategy requires the use of coated micrometric magnetic beads flowing within microfluidic channels with the starting sample to capture the EVs. Although these devices show improvements compared to bench approaches, they are typically limited to small sample volumes (typically a few microliters), in a limited working time (tens of minutes) [17,18]. The latter is mainly due to the sedimentation of the beads within the microchannels. On the other hand, most clinical studies need to process samples from hundreds of microliters to a few milliliters to investigate an appropriate number of EVs [19,20].

To fix these issues, we propose a solution based on droplet microfluidics, in which two (or more) immiscible liquids are combined by specific junctions to produce controlled emulsions of droplets of one phase dispersed in the other [21,22]. In our case, magnetic beads and starting sample containing EVs are co-encapsulated together, i) preventing the precipitation of magnetic beads within the channel regardless of the amount of sample to be analyzed or the required incubation time, and ii) improving the mixing of beads and EVs, leading to a fast EV isolation protocol. In fact, turbulence is generated spontaneously within flowing droplets, ensuring complete mixing of liquids in a few milliseconds [23,24]. A droplet microfluidic system designed to handle magnetic beads has recently been adapted for EV isolation [25]: EVs are collected and eluted from beads using a co-precipitation approach. In detail, the protocol is tested in-batch and in droplets, by analyzing 6 μL of the starting sample, reporting an improved capture efficiency (about 1.6-fold) in the second case, and a throughput of 12 μL/h.

Here, we present a novel droplet microfluidic platform that is especially designed for EV isolation, allowing higher isolation throughput (400 μL/h) and larger processable sample volume (up to 2 mL), than other microfluidics based on droplet affinity capture. The latter is a key aspect for diagnostic purposes, where between hundreds of microliters and a few milliliters of sample are analyzed [26]. Additionally, systematic comparison with a commercially available protocol shows a higher capture efficiency of about 2.5-folds for a shorter incubation time of about 4 h instead of 10 h.

This paper is organized as follows: after the description of the platform, results in terms of the microfluidic characterization and biological validation are reported and discussed. EVs from human breast cancer and canine mammary tumor cell lines are used as starting samples. A systematic comparison to the conventional ultracentrifugation approach and a commercial kit protocol is performed through protein characterization, EV quantification and imaging. Finally, isolated EVs are evaluated in terms of microRNA content.

2. Materials and methods

2.1. Droplet microfluidic experimental setup

The experimental setup specifically designed for EV purification is composed of three parts devoted to the three steps of the protocol: i) droplet generation, ii) incubation, and iii) magnetic bead extraction. Each part will be described in the following.

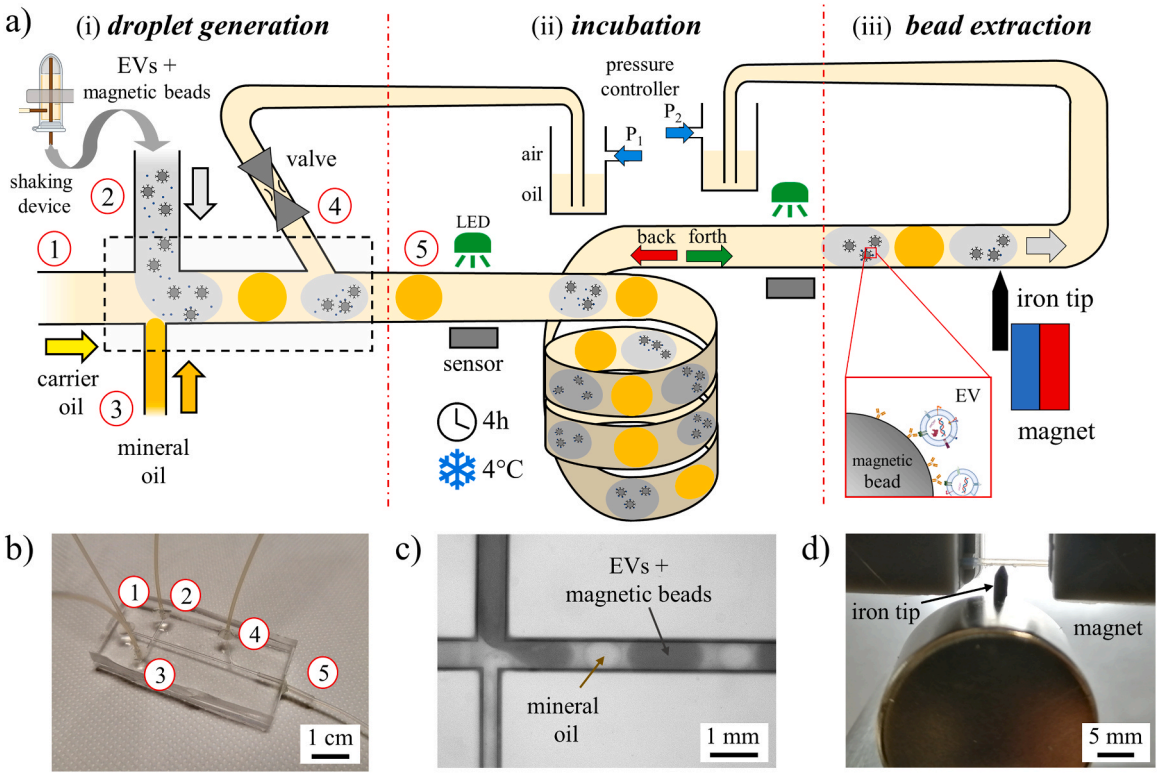

Fig. 1. (a) Complete microfluidic workflow consisting of the droplet generator, incubator, and magnetic bead extraction module. (b) Picture of the microfluidic device for droplet generation corresponding to the dashed rectangle in the upper scheme. Inlets 1, 2, and 3 are used to generate and control the motion of the droplets, while the horizontal outlet 5 allows the droplets to enter the storage capillary, preventing their break-up. Inlet 4 is connected to the pressure controller. (c) Snapshot of the droplet generation at the double T-junction: alternate aqueous phase and mineral oil droplets are generated and transported by an immiscible fluorinated oil. (d) Picture of the module for the bead extraction, with the magnetizable iron tip placed close to the magnet and in contact with the capillary transporting the droplet.

2.1.1. Setup for droplet and magnetic bead handling

A microfluidic chip presenting a double T-junction design [27] (see Fig. 1b and Section S1, Supplementary data) is used to generate alternate droplets of aqueous and mineral oil phases, dispersed in a second non-mixable carrier oil (Fig. 1c). Three syringe pumps (by Harvard Apparatus) equipped with 2.5 mL syringes (by SGE) control the flow at the inlets of the microfluidic chip through PTFE capillaries (0.5/1.0 mm ID/OD, by Sigma Aldrich). Inlet 1 is used to infuse FC-40 oil with 2% 1 H,1 H,2 H,2 H-perfluoro-1-decanol surfactant (from Sigma Aldrich) that acts as a carrier liquid, inlet 2 for the starting sample mixed with magnetic beads (Exosome-Human CD81 isolation kit, by Invitrogen), and inlet 3 for the mineral oil (by Merck Chemicals) (see Fig. 1c). The connections between the PTFE capillaries and the syringes are ensured by silicon tubing (0.5×2.5 mm ID/OD, by Deutsch and Neumann). Droplet generation is monitored by an inverted microscope (Nikon, Ti2) equipped with a camera (VEO-E, by Phantom).

Before injection into the microfluidic chip, the starting sample mixed with the magnetic beads is stored in an Eppendorf tube (0.6 or 2 mL volume) turned upside-down and coupled to a custom-made shaking device [28]. This strategy allows the complete infusion of the sample preventing any loss in the container or capillaries (see Fig. S2 in Supplementary data for more details). Once generated, droplets pass in correspondence to inlet 4 connected to a pressure controller, through a customized pinch valve [29]. This valve is used to isolate droplet generation from the incubation module. The latter consists of a capillary (0.8/1.58 mm ID/OD, by Sigma Aldrich), having a length between 1 m and 8 m, depending on the starting sample volume, placed in an ice bath (see Fig. S3d in the Supplementary data). Here, the droplets are continuously moved back-and-forth by the two pressure controllers (by Fluigent, see Fig. 1), to impose a flow rate of 30 μL/min. Two customized optical sensors are placed at the extremities of the incubation capillary to monitor the passage of droplets [30] (see Fig. S3e in the Supplementary data).

The third module is devoted to the extraction of the magnetic beads from the flowing droplets and consists of an iron tip magnetized by a permanent magnet (S-20–15-N neodymium magnet, height 1.5 cm, diameter 2 cm, grade N42, by Supermagnete) (see Fig. 1d). The iron tip has a square section (side of 1.5 mm), an edge radius of 0.12 mm, and is fixed at the center of the magnet, emerging from its edge for about 2 mm. The capillary is fixed in the vicinity of the tip by a 3D printed holder (Grey V4 resin, Form 3, by Formlabs). The bead extraction is monitored with a CMOS camera (Basler acA800–510um) equipped with a macro zoom lens (LINOS MeVis C 50 mm/f 1.8). Finally, the cluster of beads is flown out the capillary and transferred to a PCR tube (0.6 mL, by Eppendorf); then, the beads are washed twice with 500 μL of washing buffer (1x PBS, with 0.01% of BSA) and resuspended in aqueous solution for further analysis.

2.1.2. Microfluidic device production

The microfluidic chip is made of polydimethylsiloxane (PDMS, Sylgard 184, by Dow Corning) by the double replica molding technique, starting from a brass master engraved by micro-milling (by Minitech Machinery Corp.). Channel dimensions are reported in Fig. S1 of the Supplementary data. The microfluidic device is sealed by oxygen plasma and the microchannels are functionalized by flowing FC-40 with trichloro(1 H,1 H,2 H,2 H-perfluorooctyl)silane (by Alfa Aesar) 2.5% V/V for 30 minutes and then rinsed with pure FC-40.

2.2. Bead preparation for EV capturing

EV capture is provided by magnetic beads from the Exosome-Human CD81 isolation kit (by Invitrogen). Before use, beads are washed with 1 mL of phosphate buffer saline (1x PBS, by Thermo Fisher Scientific) and 0.01% of bovine serum albumin (BSA, by Sigma Aldrich). For magnetic extraction tests, beads are dispersed in double-filtered PBS solution (dfPBS) in the appropriate volume to obtain the desired concentrations. For the validation of the EV isolation of the microfluidic platform, 5×10^6 beads per 100 μL of the starting sample are used.

2.3. EV starting sample preparation

A metastatic human breast cancer cell line MDA-MB-231 and a canine primary carcinoma cell line CIPp (kindly provided by Prof. R. De Maria, University of Turin) are used. MDA-MB-231 is cultured in Dulbecco's Modified Eagle Medium 1X (by Thermo Fisher Scientific) and palm td-Tomato CIPp, generated as previously described in [31,32], and cultured in Rosewell Park Memorial Institute 1X (RPMI 1640) (by Thermo Fisher Scientific). Both culture media are supplemented with 10% Fetal Bovine Serum (FBS, by PANTM BIOTECH) and 1% penicillin/streptomycin (by Corning). Cell lines are regularly tested and confirmed to be mycoplasma-free with the Mycoalert Mycoplasma Detection kit (by Lonza). To isolate EVs, two 150 mm Petri dishes are seeded with 2.2×10^6 cells each. Cell culture medium (CCM) is replaced 24 hours before EV isolation with 25 mL of FBS-free medium.

EVs are isolated by ultracentrifugation (UC) from the cell culture medium of two plates with semi-confluent cells. The medium is first centrifuged at 300 g for 10 min at 4°C to remove any cell debris and apoptotic bodies. The supernatant is then centrifuged at 2000 g for 10 min at 4°C to remove additional debris. For the EV isolation through UC, the supernatant is transferred to a clean ultracentrifuge tube (Optima L-90 K, by Beckman Coulter) and ultracentrifuged at 100 000 g for 90 min at 4°C. The supernatant is discarded and the EV-enriched pellet is resuspended in 100 μL of double-filtered (0.2 μm) PBS (dfPBS).

For the test of the EV isolation efficacy by the droplet microfluidic platform directly from cell culture medium, the EV pellet collected after UC is spiked in 200 μL of the UC supernatant itself. Therefore, the sample results pre-concentrated but in the same starting medium.

2.4. In-batch EV isolation protocol

In-batch EV isolation is performed following the protocol suggested by the bead manufacturer (Exosome-Human CD81 isolation kit, Thermo Fisher Scientific). 80 μL of bead solution (correspondent to 10^7 beads) are transferred from the storage vial to a PCR tube and washed twice with a freshly prepared washing buffer (1 mL of 1x PBS and 0.01% of BSA). Then, 200 μL of the starting sample are added to the beads. After 10 hours of incubation in ice with end-over-end mixing, magnetic beads are extracted by the magnet. The latter is placed near the tube for 1 minute and then the supernatant is removed. The remaining beads are washed twice with 500 μL of washing buffer (1x PBS, with 0.01% of BSA) and resuspended in aqueous solution for further analysis. For the protein assay, after washing, beads are resuspended in 30 μL of radioimmunoprecipitation assay (RIPA) for the EV lysis. Differently, in the case of the Nanoparticle Tracking Analysis (NTA), the supernatant after the bead incubation is considered, before the washing steps.

2.5. EV quantification and analysis

2.5.1. Nanoparticle tracking analysis (NTA)

Samples of EVs isolated from UC and after the in-batch and microfluidic protocols are quantified in terms of particle concentration and size distribution using NanoSight NS300 (by Malvern). Aliquotes are diluted in a solution of dfPBS to obtain particles concentration between 10^7 and 10^9 particles/mL. For each sample, three 60 s movies are recorded and analyzed by 3.4 NTA software with camera level set at 12.

2.5.2. Protein content analysis by Western Blotting (WB) and Bicinchoninic Acid Assay (BCA)

Cell proteins, used as control in Western Blots, are extracted from 90% confluent cells on a 15-cm plate using 2 mL of RIPA buffer (by Thermo Fisher Scientific) supplemented with protease inhibitor according to the manufacturer's protocol.

The proteins of isolated EVs are extracted resuspending the pellet in 30 μL of RIPA buffer, supplemented with protease inhibitor. For EVs isolated from beads, the supernatant is removed from the beads by using a magnet, before EV resuspension in RIPA buffer. Samples are then sonicated for 10 seconds, incubated in ice for 15 minutes and denaturated at 70°C for 10 min on a block incubator (Dry Bath/Block Heater, by Fisherbrand).

Protein concentrations are calculated using the microBCA protein Assay Kit (by Thermo Fisher Scientific), according to the manufacturer's protocol.

For Western Blot, 20 μL of proteins are first denaturated at 70 °C for 10 min or at 95 °C for 5 min, then resolved by using Polyacrylamide Gel Electrophoresis at Neutral pH (NuPAGE) 4%–12% Bis-Tris gel (by Thermo Fisher Scientific) and transferred to a nitrocellulose membrane. Non-specific binding sites are blocked for 90 min in 5% non-fat dry milk in Tris-buffered saline containing 0.05% Tween-20 (TBS-T) at room temperature. The blots are then incubated at 4°C overnight with rabbit or mouse primary antibodies against human CD9 (1:200; by Bio-Rad MCA469GT), CD81 (1:200, by Genetex GTX101766), integrin-beta/CD29 (1:5000, by GeneTex, GTX128839) and Calnexin (1:1000; by Cell Signalling #2679). The membranes are incubated with a peroxidase-conjugate secondary antibody (1:3000; anti-Rabbit IgG #32260 or anti-Mouse IgG #32230, by Thermo Fisher Scientific) for 1 hour at room temperature. All antibodies are diluted in TBS-T containing 1% non-fat dry milk. Reactive bands are visualized using a chemiluminescent detection kit (SuperSignal West Pico PLUS Chemiluminescent Substrate, by Thermo Fisher Scientific) with the iBright instrument (by Thermo Fisher Scientific).

2.5.3. Flow cytometry analysis

Flow cytometry is performed to identify the vesicles attached to the beads using BD FACSCalibur (by BD Biosciences). At least 300 μL of the opportunely diluted sample are processed. Two different fluorescent channels are used: phycoerythrin (PE; λ_{exc_max} = 566 nm, λ_{em_max} = 576 nm) and fluorescein (FITC; λ_{exc_max} = 494 nm, λ_{em_max} = 518 nm). At least 50,000 events are acquired for each analysis.

2.5.4. Confocal microscopy

Images of EVs attached to magnetic beads are acquired by a confocal module (FV300, by Olympus) coupled to an upright microscope (BX51WI, by Olympus). The laser excitation is provided by the C-flex module with 100 mW laser head at 488 nm (by Cobolt-Hubner Photonics).

2.5.5. Quantitative Reverse Transcription Polymerase Chain reaction (qRT-PCR)

EVs isolated by the microfluidic and in-batch protocol are eluted in 700 μL of Qiazol (by Qiagen) for RNA extraction as previously reported [33]. RNA is extracted with the exoRNeasy Midi kit (by Qiagen) following the manufacturer's instructions. MiRNA retrotranscription is performed using the TaqMan™ Advanced miRNA cDNA Synthesis Kit (by Thermofisher Scientific), following the manufacturer's protocol. A fixed volume of 2 μL of RNA per reaction is used to obtain an equal load of samples, as recommended by the TaqMan™ Advanced miRNA cDNA Synthesis Kit protocol. MiRNA expression levels are evaluated by qRT-PCR with TaqMan™ Advanced miRNA assays (hsa-miR-26a-5p ID_477995_mir, hsa-miR-16a-5p ID 477860_mir, hsa-miR-21a-5p ID 477975_mir, hsa-let7a-5p ID 478575; hsa-miR-146a-5p ID 478399_mir; by Thermo Fisher Scientific). The RT reaction products are used in 5 μL PCR reactions at a final dilution of 1:10. qRT-PCR reactions are run, with 3 replicates, on a ViiA™ 7 Real-Time PCR System using these cycling conditions: hold stage for 20 sec at 95 °C; PCR stage for 1 sec at 95 °C, and 20 sec at 60 °C (for 40 cycles).

3. Results and discussion

The main results regarding the isolation of extracellular vesicles by the droplet microfluidic device will be presented and discussed below. The platform exploits the spontaneous mixing occurring within the droplets to enhance the probability of EV capture onto magnetic beads. The beads are coated with a specific antibody (anti-CD81) that acts as an anchor point for complementary proteins (CD81) typically expressed on the vesicle membrane.

The working principle of the automated protocol will first be detailed; then, the description will focus on the magnetic bead extraction and on the optimization of the overall throughput. Finally, validation of the protocol with a biological sample containing EVs will be provided in terms of particle counting, protein quantification, and miRNA content analysis.

3.1. Droplet microfluidic platform

As reported in Fig. 1, the droplet microfluidic platform developed for the isolation of EVs consists of three sequential automated modules: i) droplet generator, ii) droplet incubator and iii) magnetic beads extractor. Modules are controlled either by syringes or by pressure controllers. Before starting, the sample containing beads and EVs is initially stored in a shaking device preventing the sedimentation of beads (see Section S2 in the Supplementary data for more details). During the droplet generation through a double T-junction, the syringes are activated and the pressure difference (ΔP) of the controllers is set at zero, while the valve is kept closed to allow the droplets to move out of the PDMS chip from the outlet 5 (see Fig. 1).

The flow rates of dispersed and continuous phases can be adjusted to obtain droplets of the desired size. After proper optimization (see Section S4 in the Supplementary data), the set flow rates are 30 μL/min, 250 μL/min and 60 μL/min for carrier oil, aqueous sample and mineral oil, respectively, leading to a generation of droplets with a volume of 980±60 nL. Once the whole starting sample is divided into separated droplets, syringes are stopped, the valve is opened and the pressure controllers are activated to command the droplet motion. In detail, they are move back-and-forth during a tunable incubation time within the capillary, by alternately applying positive and negative ΔP (between 50 and 200 mbar). In particular, the generation of droplets of mineral oil in between the sample train is particularly relevant during the incubation step to prevent their merging in the case of contact [34]. Importantly, the back-and-forth motion of the droplets during incubation promotes the mixing of their content [35,36] (see Video S3 in the Supplementary data) and, consequently, is expected to foster the meeting and increase the probability of binding between EVs and beads. After incubation, the valve is closed again and the syringe connected to the inlet 1 is used to guide the droplets to the third module for the extraction of beads. Here, a magnetized metallic tip placed in proximity to the capillary allows for the extraction of beads from the parental droplets while they are flowing. Once all of the droplets are passed in front of the tip and the beads are completely captured, the generated cluster is confined to a tiny aqueous droplet. The volume of the final droplet containing the beads depends on their quantity, varying between 5 nL and 50 nL for a bead quantity between 10^4 and 10^7. The magnet is then removed and the cluster is flown out of the capillary and collected in a conventional PCR tube, prefilled with aqueous solution for subsequent EV analysis. This can be easily achieved by moving the magnetized tip away a few millimeters from the extraction region, so that magnetic beads no longer experience the magnetic force.

Above all, the entire protocol is completely automated, since all the components of the experimental platform are connected to the computer and controlled by a dedicated LabVIEW software (see Section S3 in the Supplementary data). Additionally, the microscope and cameras used to characterize microfluidic and magnetic performances of the platform are not necessary for the EV isolation itself; in fact, the customized and

low-cost optical sensors are capable of monitoring the droplet position and motion.

3.1.1. Magnetic capture efficiency characterization

The beads extraction from a parental droplet can be achieved if the magnetic force $\boldsymbol{F_M}$ acting on the beads is greater than the capillary force $\boldsymbol{F_c}$ that prevents the droplet break-up [37]. The latter can be approximated as $\boldsymbol{F_c} = \gamma \boldsymbol{L}$, where γ is the surface tension between the carrier and the droplet liquids, and $\boldsymbol{L}$ is the radius of the droplet interface to be broken. In the presented microfluidic configuration $\boldsymbol{F_c}$ can be estimated of about 6 μN (see Section S5 in Supplementary data). The magnetic force $\boldsymbol{F_M}$ experienced by magnetic beads can be approximated as:

$$\boldsymbol{F_M} \propto Q \quad \boldsymbol{M} \quad \nabla \boldsymbol{B}, \tag{1}$$

where Q and $\boldsymbol{M}$ are the number of beads inside a droplet and their magnetization vector, while $\nabla \boldsymbol{B}$ is the gradient of the applied magnetic field [37], which is affected by the shape of the magnet, in addition to its distance from the beads [38]. Given these considerations, the geometric configuration of the extraction module has been designed as shown in Fig. 2a. At first, in order to maximize $\nabla \mathbf{B}$, an iron-pointed tip (edge radius 0.12 mm) mounted on a permanent magnet is used. Compared to a flat tip with the same cross section, the pointed tip allows one to enhance the field lines near the edge of the tip, inducing a strong magnetic force that has been quantified in tens of μN by numerical simulation (see Section S5 in the Supplementary data). In fact, a flat tip would lead to a force that is one order of magnitude smaller in proximity to the edge (see Figs. S6 and S7, Supplementary data). Additionally, to minimize the distance d between the flowing droplet containing the magnetic beads and the tip, the capillary transporting the droplets is micro-engraved (see Fig. 2a,b). The wall thickness has been reduced from 390 μm to 100 μm, increasing the achievable magnetic force by five times (see Fig. S7 of the Supplementary data).

Fig. 2b shows an image sequence of the bead extraction: once the beads contained in a droplet arrive in proximity to the iron tip, they experience the magnetic force and are retained in this region, forming a cluster that is extracted from the moving droplet, which instead keeps flowing (see also Supplementary Video S1, for a droplet containing $Q = 4\times10^4$ beads). The extraction efficiency of the magnetic beads from the droplet has been evaluated as a function of the beads quantity ($Q = 10^3$-10^7 beads/droplet) and the flow rate ϕ driving the droplet (ϕ = 5–200 μL/min) (see Sections S5 and S6 of the Supplementary data for details of the bead quantification method). The results are reported in Fig. 2c, in which the extraction is considered efficient when it is greater than 90% (green star), while it is not efficient when it is between 60% and 90% (yellow diamond) or less than 60% (red cross). As expected from Eq. 1, the higher the number of beads inside the droplet, the more efficient the extraction. For the lowest rates ($\phi < 20$ μL/min), the lowest number of beads per droplet that can be extracted is about $Q = 2\times10^4$ (green area), in agreement with the numerical simulation (see Fig. S7, Supplementary data). Then, the extraction efficiency drops between

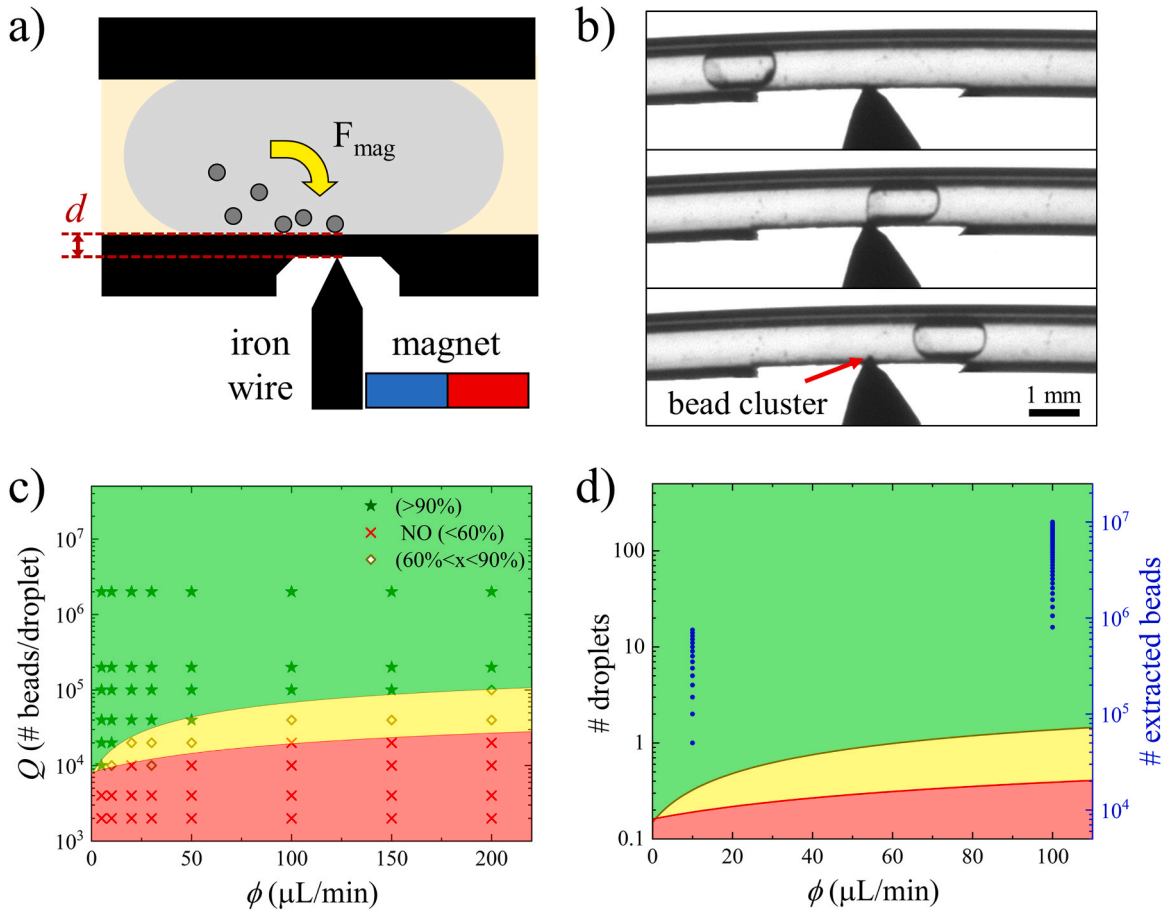

Fig. 2. (a) Schematic of the module for the extraction of magnetic beads, with the magnetizable tip in correspondence with the engraved capillary (d=100 μm) for a droplet approaching the tip; beads within the droplet experience the magnetic force F_M. (b) Image sequence of a droplet approaching (top photogram), flowing above (middle photogram) and leaving (bottom photogram) the magnetic tip; beads are extracted from the parental droplet, forming a cluster highlighted by the red arrow. (c) Experimental phase diagram of the extraction efficiency at different flow rates ϕ and magnetic bead concentrations Q. The green, yellow, and red regions correspond to extraction efficiency greater than 90%, between 60% and 90%, and lower than 60%, respectively. (d) Graph of the n-th droplet (blue dots) passing close to the tip (left vertical axis) and the number of beads extracted (right vertical axis), as a function of the applied flow rate ϕ.

60% and 90%, for $\phi > 20$ μL/min, due to the recirculation within the droplet [23]. However, for $Q > 2{\times}10^5$, the extraction efficiency is always greater than 90% for all flow rates investigated (up to 200 μL/min).

Given these results, to improve the extraction throughput of sequentially flowing droplets containing $Q = 5{\times}10^4$ beads, the applied flow rate is kept fixed at 10 μL/min for the first 15 droplets and increased up to 100 μL/min from the 16th (see also the Supplementary Video S2). In fact, the accumulation of the extracted beads forming a gradually increasing cluster allows the flow rate to increase without affecting the extraction efficiency (> 90%), as shown in Fig. 2d, where the droplet number (left vertical axis) and the related accumulated beads (right vertical axis) are plotted as functions of the applied flow rate. Importantly, this method allows handling a wide range of sample volumes from few μL up to mL in less than half an hour.

3.1.2. *Throughput quantification of the droplet platform*

To assess the throughput of the droplet microfluidic platform for different starting sample volumes (V = 50–2000 μL), the purification experiment is carried out measuring the time contribution of each module (see Fig. 3): droplet generation (orange), incubation (white) and beads extraction (grey). The generation of droplets is obtained by keeping constant the applied flow rates for the oils and bead suspension phase, and thus, its time contribution increases linearly with V, taking about 10 minutes for 2 mL. Similarly, apart from the first 15 droplets flown at 10 μL/min (processed in appoximately 2 minutes), the extraction time also increases linearly with the sample volume, taking approximately 25 minutes for 2 mL (see Section S7 of the Supplementary data for more details). A fixed incubation time of 4 hours is used for all volumes; this time is shorter than that required by the conventional EV purification protocol but sufficiently long to allow the formation of the chemical antibody-antigen bond (see Section 3.2).

Therefore, Fig. 3 proves that the microfluidic platform can handle large sample volumes (tested up to 2 mL) and lead to high-throughput analysis (4.5 hours for 2 mL, corresponding to approximately 450 μL/h). This could be achieved by exploiting droplets that allow decoupling the handling of the EVs and beads from their incubation. Additionally, compared to the previously reported droplet device, throughput improves about 40 times [25].

3.2. *Validation of the EV isolation*

To validate the microfluidic platform, EVs obtained from a breast cancer cell line (MDA-MB-231) resuspended in 200 μL of phosphate buffer saline (PBS) are considered. This starting sample is then loaded

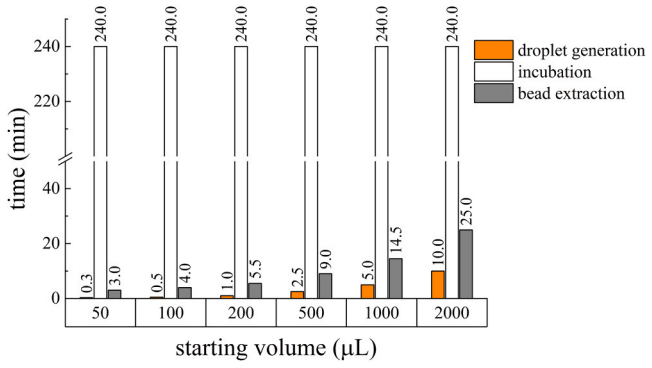

Fig. 3. Stacked bar chart of the percentage time intervals required for droplet generation (orange), incubation (white) and magnetic bead extraction (grey), considering the entire microfluidic protocol. In the bars, each contribution of the time interval is also reported in minutes; while the incubation time is constant (240 minutes), the generation and extraction times depend on the amount of starting sample.

with about 10^7 magnetic beads coated with CD81 antibody and processed using two distinct protocols: one based on the microfluidic platform and the other set by the manufacturer of the beads (in-batch). In the latter case, the sample protocol requires an overnight incubation on a mixer at 4°C. After their magnetic extraction, the beads and the remaining supernatant are collected for subsequent analysis. Since the designed microfluidic platform aims to be a general tool for EV purification, its performance is evaluated considering: i) protein quantification and recognition, ii) EV capture efficiency, defined as the ratio between the isolated EVs and their initial quantity, and iii) microRNA cargo availability for further diagnostic applications.

To assess the influence of the incubation time during the microfluidic protocol, the protein concentration of the isolated EVs is quantified by the bicinchoninic acid (BCA) assay. Different incubation times (1, 4 and 8 hours) are tested by the microfluidic approach and compared with the bead manufacturer's protocol (in-batch). Fig. 4a shows that the protein concentration after 1 hour of incubation is lower than that obtained from the in-batch protocol (overnight incubation, 10 hours). In contrast, 4-hour and 8-hour incubations show similar protein amounts, and, more surprisingly, higher than after in-batch incubation. Therefore, 4 hours represent a sufficient incubation time for the EVs to be captured by magnetic beads within droplets and, based on the protein quantitation, the capture efficiency results improved by approximately 2.4-folds compared to the in-batch protocol.

To characterize the protein from the isolated EVs, western blot (WB) analyses are performed (see Fig. 4b and Fig. S10 in the Supplementary data). The most representative proteins for EV characterization are analyzed (transmembrane proteins: CD9, CD81, integrin-β) [39,40], while calnexin is used as a negative control [41]. The first column reports the protein expression in the cell line from which the EVs are isolated and, as expected, all proteins are well represented. Samples from both in-batch and microfluidic protocols exhibit the same bands from transmembrane proteins as those from the starting sample, which means that part of the EVs expressing these membrane markers are captured. The fact that the signals after purification are weaker compared to the starting sample may suggest the loss of some vesicles. In any case, the WB signals from the microfluidic protocol are slightly stronger than those from the in-batch protocol, in agreement with the results from the BCA analysis. This is probably due to the more efficient mixing occurring within the droplets than within the conventional tube, where beads typically tend to sediment at the bottom of the tube during the incubation. Differently, within the droplets both beads and EVs are continuously agitated, increasing their binding probability (see Video S3 in the Supplementary data).

To further quantify the capture efficiency of EVs, Nanoparticle Tracking Analysis (NTA) is performed on the starting sample and on the supernatant after isolation, both in-batch and in droplets (see Fig. 5, and Fig. S11 in the Supplementary data). As already used in [42], quantification from the supernatant is required, as EVs cannot be detached from the magnetic beads after capture. In detail, for the in-batch protocol, the supernatant after the EV-bead incubation is considered. In the case of the microfluidic experiment, the supernatant is collected by gathering all droplets at the outlet of the capillary after bead extraction. In this way, the two supernatants can be directly compared. The capture efficiency is calculated as: $\text{capture efficiency}(\%) = [1 - (\text{conc.supernatant})/(\text{conc.sample})] \times 100$.

As shown in Fig. 5 and by the data reported below, the comparison between the mean values of three NTA recordings shows an EV capture efficiency of 22% for the in-batch protocol, and of 56% for the microfluidic platform. Thus, an improvement of a factor of 2.5 is observed, which confirms the BCA results.

Qualitative evaluation of EV presence onto magnetic beads is provided by flow cytometry (see Fig. 6a). For this analysis, EVs isolated from the CIPp canine cell line fluorescently tagged with td-Tomato [32] are used as the starting sample. As typically performed [32], two different fluorescent channels are recorded: phycoerythrin (PE), which

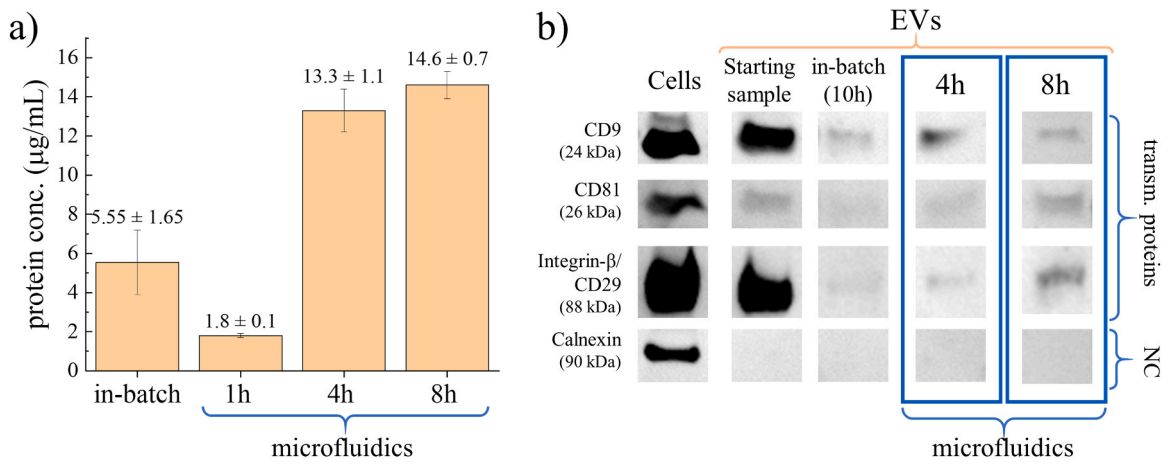

Fig. 4. (a) Total protein concentration derived from different isolation protocols evaluated by microBCA assay; three incubation times (1 h, 4 h and 8 h) are evaluated by the microfluidic platform. Data results from the average of three independent experiments and error bars are the related standard deviations. (b) Western blot of five different samples: cell line-lysate, starting EV sample obtained by UC and, after in-batch and microfluidic (4 h and 8 h) isolation protocols.

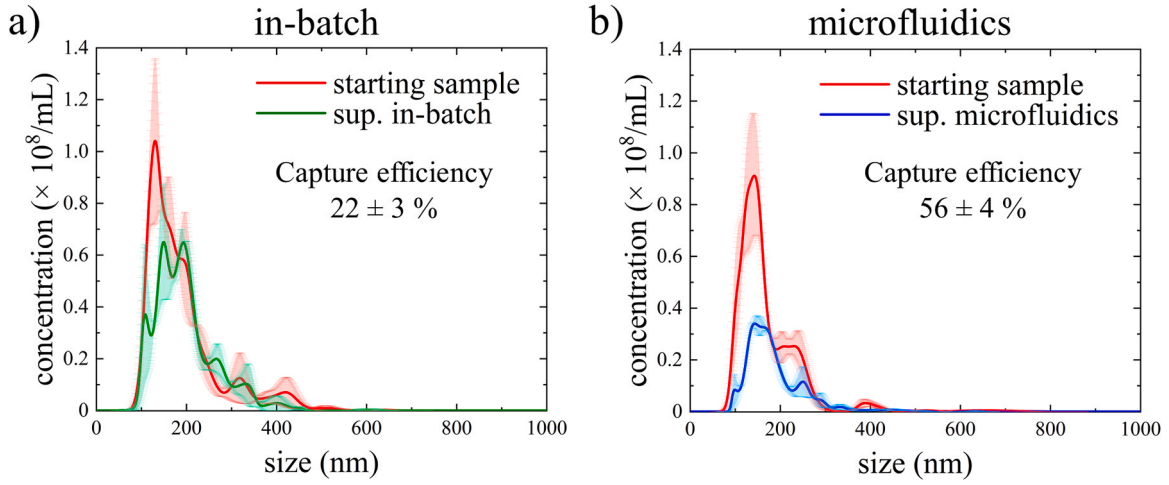

	Conc. (10^9/ml)	Size (nm)
Sample	10.7 ± 0.6	190 ± 11
Supernatant	8.3 ± 0.5	196 ± 10

	Conc. (10^9/ml)	Size (nm)
Sample	8.2 ± 0.7	173 ± 8
Supernatant	3.6 ± 0.5	187 ± 3

Fig. 5. NTA results of the EV size distribution from three different assays after (a) droplet microfluidic or (b) in-batch isolation, compared to their respective starting sample. A table with the mean values of both the EV concentration and the size of the starting sample and the supernatants after the two protocols is also reported.

matches the emission band of the EV, and fluorescein (FITC) as a control to filter the noisy background from bead scattering. Thus, the upper left region of the flow cytometry scatterplot identifies the PE-positive beads, covered by the tdTomato-positive EVs. Fig. 6a compares the data of the beads isolated from the in-batch protocol with those obtained from the microfluidic platform (4-hour incubation). As a negative control, data from the sample containing only beads are also reported. Similar results are found using the two purification methods. The small counting rate, typically observed for this type of measurements [43], is probably due to the presence of dark micrometric beads that can shield both excitation and emission light, decreasing the optical signal. Therefore, not all the EVs attached to the beads are expected to be detectable. Finally, confocal images confirm the presence of EVs attached to the magnetic beads: the bright field image (Fig. 6b,left) reports the magnetic beads and the fluorescent image (Fig. 6b,right) shows the EVs on their surface.

The integrity of isolated EVs is further investigated by analyzing their genomic content. In fact, unlike proteins that are present in the EV membrane, miRNAs are usually collected within the vesicle matrix. Thus, non-intact EVs are expected to lose their miRNAs cargo in the supernatant, being not capturable by the beads; differently, EVs that maintain their integrity still carry the miRNAs. The miRNA is obtained from both in-batch and microfluidic samples and then retrotranscribed for quantitative RT-PCR analysis. The presence of some commonly expressed miRNAs in the MDA-MB-231 breast cancer cell line (miR-26a-5p, miR-16–5p, miR-21–5p, miR-let7a-5p, and miR-146a-5p) is investigated [44–46]. The mean C_T values obtained by PCR analysis are between 23 and 28 (see Table S1 in the Supplementary data), which shows a significant presence of miRNA in the sample and thus demonstrates the integrity of the isolated EVs [47]. Additionally, similar C_T values are obtained from both microfluidic and in-batch isolations, indicating that the mixing within the droplets does not damage the EVs.

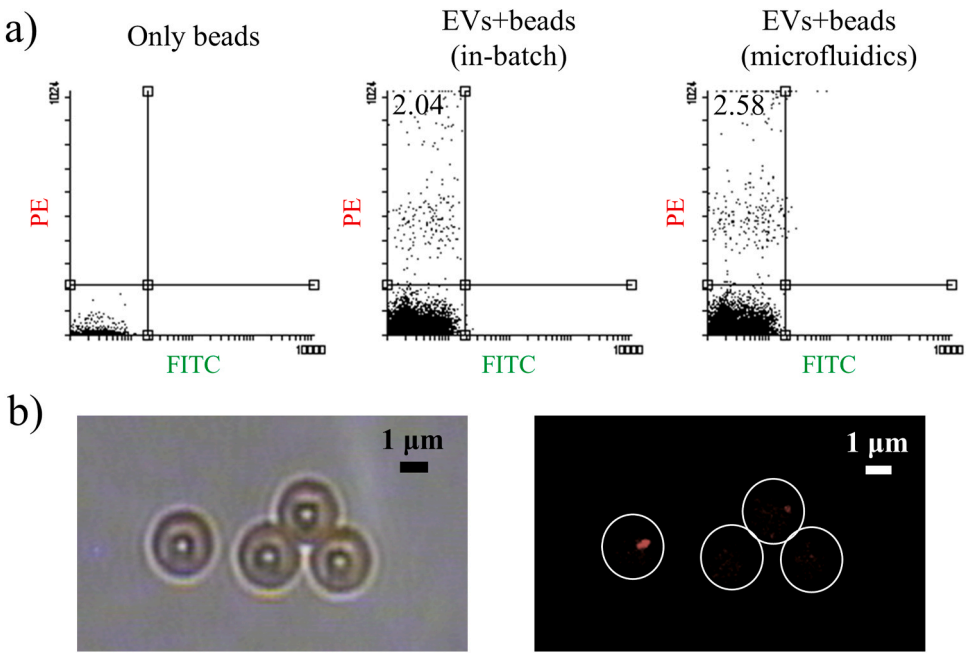

Fig. 6. (a) Flow cytometric evaluation of the bare magnetic beads (left), and of beads having attached EVs after in-batch (center) or microfluidic isolation (right) protocols, showing comparable capture efficiencies, respectively, of 2.04% and 2.58%. b) Images of EV-bead complexes acquired by confocal microscopy in the bright field (left) and in fluorescence (right), where continuous white lines corresponding to the boundaries of the beads are drawn as an eye guide. The red signals within the boundaries are the fluorescence provided by the EVs.

3.3. EV isolation from cell culture medium

Finally, to increase the level of complexity of the purification assay performed by the microfluidic platform and verify its capability, EVs are also isolated directly from the cell culture medium of the MDA-MB-231 cell lines, after removing cell debris. Importantly, this test allows understanding whether the ultracentrifugation step is required to isolate the EVs by droplet microfluidics. In fact, unlike the previously reported results in which EVs are dispersed in PBS after ultracentrifugation, cell culture medium can contain free proteins or small agglomerations that may affect droplet handling and the capture on the beads. Western Blot analysis shows that all investigated transmembrane proteins are present with a signal intensity similar to that of the starting sample (see Fig. S12 in the Supplementary data). Therefore, EV isolation from the droplet microfluidic platform is also possible from more complex samples, such as cell culture medium.

4. Conclusion

In this study, we present and validate a novel platform based on droplet microfluidics and magnetic beads handling to isolate extracellular vesicles. Notably, the use of droplet microfluidics allows for an improvement in the capture efficiency of 2.5-fold within a shorter incubation time than for the same protocol performed in batch. Additionally, remarkable improvements in terms of sample volume (up to 2 mL of starting sample) and analysis throughput (more than 400 µL/h), with respect to monophasic microfluidic devices are achieved. In fact, the latter are strongly limited by bead sedimentation. Because of their size (1–3 µm) and higher density (1.4–1.8 g/cm^3 [48]) compared to the carrier liquid (~1.0 g/cm^3), beads sediment approximately two orders of magnitude faster than EVs, which are 100 times smaller and almost density matched with the surrounding aqueous phase [13]. As a consequence, in monophasic microfluidics, specific flow rates are required: the flow rates must be high enough to make the bead sedimentation negligible while slow enough to promote the EV capture on the bead surface. For that, in monophasic microfluidics, typical throughputs are between 0.1 and 0.5 µL/min [17,18], and especially, the highest processable volume is of hundreds of µL, while, the presented droplet microfluidic platform has been validated up to 7 of µL/min and 2 mL of starting sample. This improvement is due to the decoupling of magnetic bead handling from the incubation required for EV capturing. The encapsulation of beads and EVs in droplets is performed quickly (between 20 sec and 10 min), making the sedimentation of beads negligible. Differently, the incubation time can be tuned independently of the previous step, since beads cannot escape the droplet interface and are, in fact, continuously agitated. The only other existing droplet microfluidic system tested for EV isolation reports a better capture efficiency than the same protocol performed in-batch, analyzing 6 µL of sample with a throughput of about 12 µL/h [25]. It should be noted that the throughput of our droplet platform (400 µL/h) is currently limited by the incubation step (currently 4 hours), representing 90% of the overall protocol time. However, since this duration is related to the antigen-antibody reaction, optimization of the bead coating could allow further increase in total throughput [49,50]. In the present study, commercially available beads have been used to perform a systematic comparison with an existing and diffuse protocol. However, customized beads can also be considered to reduce the cost of the required reagents [51], or other affinity capture approaches to promote EV elution after isolation [25,52], currently limited by the employed antigen-antibody reaction.

Based on these achievements, we believe that the use of droplet microfluidics for EV isolation shows great potential for both fundamental studies and clinical applications, where hundreds of µL to a few mL of starting sample must be considered [26]. However, for clinical sample handling (e.g. plasma or serum) devoted optimization might be required in terms of surfactants to assure droplets stability, as well as on the magnetic bead coating for immunocapturing [53].

CRediT authorship contribution statement

Giampaolo Mistura: Methodology, Supervision, Writing – original draft, Writing – review & editing. **Valentina Zappulli:** Conceptualization, Funding acquisition, Resources, Supervision, Writing – original draft, Writing – review & editing. **Lara Mussolin:** Funding acquisition,

Resources, Supervision, Writing – original draft. **Matteo Pierno:** Conceptualization, Funding acquisition, Methodology, Resources, Supervision, Writing – original draft, Writing – review & editing. **Carlotta Caterina Damanti:** Data curation, Formal analysis, Methodology. **Beatrice Crestani:** Data curation, Formal analysis, Methodology. **Alessandro Sammarco:** Investigation, Methodology. **Paola Brun:** Conceptualization, Data curation, Formal analysis, Funding acquisition. **Valentina Moccia:** Data curation, Methodology, Writing – original draft, Writing – review & editing. **Davide Ferraro:** Conceptualization, Data curation, Formal analysis, Funding acquisition, Methodology, Project administration, Supervision, Validation, Writing – original draft, Writing – review & editing. **Alessio Meggiolaro:** Conceptualization, Data curation, Methodology, Validation, Writing – original draft, Writing – review & editing.

Declaration of Competing Interest

The authors declare that they have no known competing financial interests or personal relationships that could have appeared to influence the work reported in this paper.

Data Availability

Data will be made available on request.

Acknowledgements

The authors acknowledge Dr. Ilaria Fortunati and Prof. Camilla Ferrante for confocal microscopy; Giorgio Delfitto for technical assistance; Maria Poles for experimental contribution for protein analysis. This research was funded by the University of Padova through the STARS grant (EXODROP), the BIRD grant 2021 (BiodivSeq), the Associazione Italiana per la Ricerca sul Cancro, Milan, (Investigator Grants - IG 2018#21385 to L.M.) We acknowledge financial support under the National Recovery and Resilience Plan (NRRP), Mission 4, Component 2, Investment 1.1, calls No. 104 (2.2.2022) and No. 1409 (14.9.2022) by the Italian Ministry of University and Research (MUR), funded by the European Union – NextGenerationEU– for the Projects OCEAN (CUP C53D23000790006; No. 2022YYLSJ2) and EXTREME (CUP G53D23007030001; No. P2022J2ZC2) adopted by the Italian Ministry of Ministry of University and Research (MUR).

Supplementary data

Supplementary data to this article can be found online at XXX

Received: ((will be filled in by the editorial staff))
Revised: ((will be filled in by the editorial staff))
Published online: ((will be filled in by the editorial staff))

Appendix A. Supporting information

Supplementary data associated with this article can be found in the online version at doi:10.1016/j.snb.2024.135583.

References

[1] C. Théry, K.W. Witwer, E. Aikawa, M.J. Alcaraz, J.D. Anderson, R. Andriantsitohaina, A. Antoniou, T. Arab, F. Archer, G.K. Atkin-Smith, D.C. Ayre, J.M. Bach, D. Bachurski, H. Baharvand, L. Balaj, S. Baldacchino, N.N. Bauer, A. A. Baxter, M. Bebawy, C. Beckham, A. Bedina Zavec, A. Benmoussa, A.C. Berardi, P. Bergese, E. Bielska, C. Blenkiron, S. Bobis-Wozowicz, E. Boilard, W. Boireau, A. Bongiovanni, F.E. Borràs, S. Bosch, C.M. Boulanger, X. Breakefield, A.M. Breglio, M. Brennan, D.R. Brigstock, A. Brisson, M.L.D. Broekman, J.F. Bromberg, P. Bryl-Górecka, S. Buch, A.H. Buck, D. Burger, S. Busatto, D. Buschmann, B. Bussolati, E. I. Buzás, J.B. Byrd, G. Camussi, D.R.F. Carter, S. Caruso, L.W. Chamley, Y.T. Chang, A.D. Chaudhuri, C. Chen, S. Chen, L. Cheng, A.R. Chin, A. Clayton, S.P. Clerici, A. Cocks, E. Cocucci, R.J. Coffey, A. Cordeiro-da-Silva, Y. Couch, F.A.W. Coumans, B. Coyle, R. Crescitelli, M.F. Criado, C. D'Souza-Schorey, S. Das, P. de Candia, E. F. De Santana, O. De Wever, H.A. del Portillo, T. Demaret, S. Deville, A. Devitt, B. Dhondt, D. Di Vizio, L.C. Dieterich, V. Dolo, A.P. Dominguez Rubio, M. Dominici, M.R. Dourado, T.A.P. Driedonks, F.V. Duarte, H.M. Duncan, R. M. Eichenberger, K. Ekström, S.E.L. Andaloussi, C. Elie-Caille, U. Erdbrügger, J. M. Falcón-Pérez, F. Fatima, J.E. Fish, M. Flores-Bellver, A. Försönits, A. Frelet-Barrand, F. Fricke, G. Fuhrmann, S. Gabrielsson, A. Gámez-Valero, C. Gardiner, K. Gärtner, R. Gaudin, Y.S. Gho, B. Giebel, C. Gilbert, M. Gimona, I. Giusti, D.C. I. Goberdhan, A. Görgens, S.M. Gorski, D.W. Greening, J.C. Gross, A. Gualerzi, G. N. Gupta, D. Gustafson, A. Handberg, R.A. Haraszti, P. Harrison, H. Hegyesi, A. Hendrix, A.F. Hill, F.H. Hochberg, K.F. Hoffmann, B. Holder, H. Holthofer, B. Hosseinkhani, G. Hu, Y. Huang, V. Huber, S. Hunt, A.G.E. Ibrahim, T. Ikezu, J. M. Inal, M. Isin, A. Ivanova, H.K. Jackson, S. Jacobsen, S.M. Jay, M. Jayachandran, G. Jenster, L. Jiang, S.M. Johnson, J.C. Jones, A. Jong, T. Jovanovic-Talisman, S. Jung, R. Kalluri, S. ichi Kano, S. Kaur, Y. Kawamura, E.T. Keller, D. Khamari, E. Khomyakova, A. Khvorova, P. Kierulf, K.P. Kim, T. Kislinger, M. Klingeborn, D. J. Klinke, M. Kornek, M.M. Kosanović, Á.F. Kovács, E.M. Krämer-Albers, S. Krasemann, M. Krause, I.V. Kurochkin, G.D. Kusuma, S. Kuypers, S. Laitinen, S. M. Langevin, L.R. Languino, J. Lannigan, C. Lässer, L.C. Laurent, G. Lavieu, E. Lázaro-Ibáñez, S. Le Lay, M.S. Lee, Y.X.F. Lee, D.S. Lemos, M. Lenassi, A. Leszczynska, I.T.S. Li, K. Liao, S.F. Libregts, E. Ligeti, R. Lim, S.K. Lim, A. Linē, K. Linnemannstöns, A. Llorente, C.A. Lombard, M.J. Lorenowicz, Á.M. Lörincz, J. Lötvall, J. Lovett, M.C. Lowry, X. Loyer, Q. Lu, B. Lukomska, T.R. Lunavat, S.L. N. Maas, H. Malhi, A. Marcilla, J. Mariani, J. Mariscal, E.S. Martens-Uzunova, L. Martin-Jaular, M.C. Martinez, V.R. Martins, M. Mathieu, S. Mathivanan, M. Maugeri, L.K. McGinnis, M.J. McVey, D.G. Meckes, K.L. Meehan, I. Mertens, V. R. Minciacchi, A. Möller, M. Møller Jørgensen, A. Morales-Kastresana, J. Morhayim, F. Mullier, M. Muraca, L. Musante, V. Mussack, D.C. Muth, K. H. Myburgh, T. Najrana, M. Nawaz, I. Nazarenko, P. Nejsum, C. Neri, T. Neri, R. Nieuwland, L. Nimrichter, J.P. Nolan, E.N.M. Nolte-'t Hoen, N. Noren Hooten, L. O'Driscoll, T. O'Grady, A. O'Loghlen, T. Ochiya, M. Olivier, A. Ortiz, L.A. Ortiz, X. Osteikoetxea, O. Ostegaard, M. Ostrowski, J. Park, D.M. Pegtel, H. Peinado, F. Perut, M.W. Pfaffl, D.G. Phinney, B.C.H. Pieters, R.C. Pink, D.S. Pisetsky, E. Pogge von Strandmann, I. Polakovicova, I.K.H. Poon, B.H. Powell, I. Prada, L. Pulliam, P. Quesenberry, A. Radeghieri, R.L. Raffai, S. Raimondo, J. Rak, M. I. Ramirez, G. Raposo, M.S. Rayyan, N. Regev-Rudzki, F.L. Ricklefs, P.D. Robbins, D.D. Roberts, S.C. Rodrigues, E. Rohde, S. Rome, K.M.A. Rouschop, A. Rughetti, A. E. Russell, P. Saá, S. Sahoo, E. Salas-Huenuleo, C. Sánchez, J.A. Saugstad, M.J. Saul, R.M. Schiffelers, R. Schneider, T.H. Schøyen, A. Scott, E. Shahaj, S. Sharma, O. Shatnyeva, F. Shekari, G.V. Shelke, A.K. Shetty, K. Shiba, P.R.M. Siljander, A. M. Silva, A. Skowronek, O.L. Snyder, R.P. Soares, B.W. Sódar, C. Soekmadji, J. Sotillo, P.D. Stahl, W. Stoorvogel, S.L. Stott, E.F. Strasser, S. Swift, H. Tahara, M. Tewari, K. Timms, S. Tiwari, R. Tixeira, M. Tkach, W.S. Toh, R. Tomasini, A. C. Torrecilhas, J.P. Tosar, V. Toxavidis, L. Urbanelli, P. Vader, B.W.M. van Balkom, S.G. van der Grein, J. Van Deun, M.J.C. van Herwijnen, K. Van Keuren-Jensen, G. van Niel, M.E. van Royen, A.J. van Wijnen, M.H. Vasconcelos, I.J. Vechetti, T. D. Veit, L.J. Vella, É. Velot, F.J. Verweij, B. Vestad, J.L. Viñas, T. Visnovitz, K. V. Vukman, J. Wahlgren, D.C. Watson, M.H.M. Wauben, A. Weaver, J.P. Webber, V. Weber, A.M. Wehman, D.J. Weiss, J.A. Welsh, S. Wendt, A.M. Wheelock, Z. Wiener, L. Witte, J. Wolfram, A. Xagorari, P. Xander, J. Xu, X. Yan, M. Yáñez-Mó, H. Yin, Y. Yuana, V. Zappulli, J. Zarubova, V. Žėkas, J. ye Zhang, Z. Zhao, L. Zheng, A.R. Zheutlin, A.M. Zickler, P. Zimmermann, A.M. Zivkovic, D. Zocco, E. K. Zuba-Surma, Minimal information for studies of extracellular vesicles 2018 (MISEV2018): a position statement of the International Society for Extracellular Vesicles and update of the MISEV2014 guidelines, J. Extracell. Vesicles. 7 (2018), https://doi.org/10.1080/20013078.2018.1535750.

[2] G. Raposo, W. Stoorvogel, Extracellular vesicles: exosomes, microvesicles, and friends, J. Cell Biol. 200 (2013) 373–383, https://doi.org/10.1083/jcb.201211138.

[3] G. Raposo, P.D. Stahl, Extracellular vesicles: a new communication paradigm? Nat. Rev. Mol. Cell Biol. 20 (2019) 509–510, https://doi.org/10.1038/s41580-019-0158-7.

[4] L. Zhao, W. Liu, J. Xiao, B. Cao, The role of exosomes and "exosomal shuttle microRNA" in tumorigenesis and drug resistance, Cancer Lett. 356 (2015) 339–346, https://doi.org/10.1016/J.CANLET.2014.10.027.

[5] F. Momen-Heravi, L. Balaj, S. Alian, P.Y. Mantel, A.E. Halleck, A.J. Trachtenberg, Current methods for the isolation of extracellular vesicles, Biol. Chem. 394 (2013) 1253–1262, https://doi.org/10.1515/hsz-2013-0141.

[6] S. Gandham, X. Su, J. Wood, A.L. Nocera, S.C. Alli, L. Milane, A. Zimmerman, M. Amiji, A.R. Ivanov, Technologies and standardization in research on extracellular vesicles, Trends Biotechnol. 38 (2020) 1066–1098, https://doi.org/10.1016/j.tibtech.2020.05.012.

[7] M. Yáñez-Mó, P.R.M. Siljander, Z. Andreu, A.B. Zavec, F.E. Borràs, E.I. Buzas, K. Buzas, E. Casal, F. Cappello, J. Carvalho, E. Colás, A. Cordeiro-Da Silva, S. Fais, J.M. Falcon-Perez, I.M. Ghobrial, B. Giebel, M. Gimona, M. Graner, I. Gursel, M. Gursel, N.H.H. Heegaard, A. Hendrix, P. Kierulf, K. Kokubun, M. Kosanovic, V. Kralj-Iglic, E.M. Krämer-Albers, S. Laitinen, C. Lässer, T. Lener, E. Ligeti, A. Line, G. Lipps, A. Llorente, J. Lötvall, M. Manček-Keber, A. Marcilla, M. Mittelbrunn, I. Nazarenko, E.N.M. Nolte-'t Hoen, T.A. Nyman, L. O'Driscoll, M. Olivan, C. Oliveira, É. Pállinger, H.A. Del Portillo, J. Reventós, M. Rigau, E. Rohde, M. Sammar, F. Sánchez-Madrid, N. Santarém, K. Schallmoser, M.S. Ostenfeld, W. Stoorvogel, R. Stukelj, S.G. Van Der Grein, M. Helena Vasconcelos, M.H. M. Wauben, O. De Wever, Biological properties of extracellular vesicles and their physiological functions, J. Extracell. Vesicles. 4 (2015) 1–60, https://doi.org/10.3402/jev.v4.27066.

[8] X. Fang, C. Chen, B. Liu, Z. Ma, F. Hu, H. Li, H. Gu, H. Xu, A magnetic bead-mediated selective adsorption strategy for extracellular vesicle separation and

purification, Acta Biomater. 124 (2021) 336–347, https://doi.org/10.1016/j.actbio.2021.02.004.
[9] Y.T. Kang, E. Purcell, C. Palacios-Rolston, T.W. Lo, N. Ramnath, S. Jolly, S. Nagrath, Isolation and profiling of circulating tumor-associated exosomes using extracellular vesicular lipid–protein binding affinity based microfluidic device, Small 15 (2019) 1–14, https://doi.org/10.1002/smll.201903600.
[10] J. Park, J.S. Park, C.H. Huang, A. Jo, K. Cook, R. Wang, H.Y. Lin, J. Van Deun, H. Li, J. Min, L. Wang, G. Yoon, B.S. Carter, L. Balaj, G.S. Choi, C.M. Castro, R. Weissleder, H. Lee, An integrated magneto-electrochemical device for the rapid profiling of tumour extracellular vesicles from blood plasma, Nat. Biomed. Eng. 5 (2021) 678–689, https://doi.org/10.1038/s41551-021-00752-7.
[11] Y.H. Soung, S. Ford, V. Zhang, J. Chung, Exosomes in cancer diagnostics, Cancers (Basel) 9 (2017), https://doi.org/10.3390/cancers9010008.
[12] P. Mitchell, Microfluidics—downsizing large-scale biology, Nat. Biotechnol. 19 (2001) 717–721. ⟨https://www.nature.com/articles/nbt0801_717⟩.
[13] A. Meggiolaro, V. Moccia, P. Brun, M. Pierno, G. Mistura, V. Zappulli, D. Ferraro, Microfluidic strategies for extracellular vesicle isolation: towards clinical applications, Biosensors 13 (2023) 1–33, https://doi.org/10.3390/bios13010050.
[14] S.S. Kanwar, C.J. Dunlay, D.M. Simeone, S. Nagrath, Microfluidic device (ExoChip) for on-chip isolation, quantification and characterization of circulating exosomes, Lab Chip 14 (2014) 1891–1900, https://doi.org/10.1039/c4lc00136b.
[15] Z. Wang, H.J. Wu, D. Fine, J. Schmulen, Y. Hu, B. Godin, J.X.J. Zhang, X. Liu, Ciliated micropillars for the microfluidic-based isolation of nanoscale lipid vesicles, Lab Chip 13 (2013) 2879–2882, https://doi.org/10.1039/c3lc41343h.
[16] P. Zhang, X. Zhou, M. He, Y. Shang, A.L. Tetlow, A.K. Godwin, Y. Zeng, Ultrasensitive detection of circulating exosomes with a 3D-nanopatterned microfluidic chip, Nat. Biomed. Eng. 3 (2019) 438–451, https://doi.org/10.1038/s41551-019-0356-9.
[17] Z. Zhao, Y. Yang, Y. Zeng, M. He, A microfluidic ExoSearch chip for multiplexed exosome detection towards blood-based ovarian cancer diagnosis, Lab Chip 16 (2016) 489–496, https://doi.org/10.1039/c5lc01117e.
[18] M. He, J. Crow, M. Roth, Y. Zeng, A.K. Godwin, Integrated immunoisolation and protein analysis of circulating exosomes using microfluidic technology, Lab Chip 14 (2014) 3773–3780, https://doi.org/10.1039/c4lc00662c.
[19] I.V. Bijnsdorp, O. Maxouri, A. Kardar, T. Schelfhorst, S.R. Piersma, T.V. Pham, A. Vis, R.J. Van Moorselaar, C.R. Jimenez, Feasibility of urinary extracellular vesicle proteome profiling using a robust and simple, clinically applicable isolation method, J. Extracell. Vesicles. 6 (2017), https://doi.org/10.1080/20013078.2017.1313091.
[20] D. Zocco, S. Bernardi, M. Novelli, C. Astrua, P. Fava, N. Zarovni, F.M. Carpi, L. Bianciardi, O. Malavenda, P. Quaglino, C. Foroni, D. Russo, A. Chiesi, M. T. Fierro, Isolation of extracellular vesicles improves the detection of mutant DNA from plasma of metastatic melanoma patients, Sci. Rep. 10 (1) (2020) 12, https://doi.org/10.1038/s41598-020-72834-6.
[21] C.N. Baroud, F. Gallaire, R. Dangla, Dynamics of microfluidic droplets, Lab Chip 10 (2010) 2032–2045, https://doi.org/10.1039/c001191f.
[22] T.S. Kaminski, P. Garstecki, Controlled droplet microfluidic systems for multistep chemical and biological assays, Chem. Soc. Rev. 46 (2017) 6210–6226, https://doi.org/10.1039/c5cs00717h.
[23] H. Song, M.R. Bringer, J.D. Tice, C.J. Gerdts, R.F. Ismagilov, Experimental test of scaling of mixing by chaotic advection in droplets moving through microfluidic channels, Appl. Phys. Lett. 83 (2003) 4664–4666, https://doi.org/10.1063/1.1630378.
[24] H. Song, D.L. Chen, R.F. Ismagilov, Reactions in droplets in microfluidic channels, Angew. Chem. - Int. Ed. 45 (2006) 7336–7356, https://doi.org/10.1002/anie.200601554.
[25] M. Morani, M. Taverna, Z. Krupova, L. Alexandre, P. Defrenaix, T.D. Mai, Development of a microfluidic droplet platform with an antibody-free magnetic-bead-based strategy for high through-put and efficient EVs isolation, Talanta 249 (2022) 123625, https://doi.org/10.1016/j.talanta.2022.123625.
[26] R.E. Veerman, L. Teeuwen, P. Czarnewski, G. Güclüler Akpinar, A.S. Sandberg, X. Cao, M. Pernemalm, L.M. Orre, S. Gabrielsson, M. Eldh, Molecular evaluation of five different isolation methods for extracellular vesicles reveals different clinical applicability and subcellular origin, J. Extracell. Vesicles. 10 (2021), https://doi.org/10.1002/jev2.12128.
[27] J.H. Xu, S.W. Li, J. Tan, Y.J. Wang, G.S. Luo, Preparation of highly monodisperse droplet in a T-junction microfluidic device, AIChE J. 52 (2006) 3005–3010, https://doi.org/10.1002/aic.10924.
[28] M. Poles, A. Meggiolaro, S. Cremaschini, M. Pierno, G. Mistura, D. Ferraro, F. Marinello, D. Filippi, Shaking device for homogeneous dispersion of magnetic beads in droplet microfluidics, Sensors 23 (2023) 5399, https://doi.org/10.3390/s23125399.
[29] D. Ferraro, M. Serra, I. Ferrante, J.L. Viovy, S. Descroix, Microfluidic valve with zero dead volume and negligible back-flow for droplets handling, Sens. Actuators, B Chem. 258 (2018) 1051–1059, https://doi.org/10.1016/j.snb.2017.12.002.
[30] D. Ferraro, M. Serra, D. Filippi, L. Zago, E. Guglielmin, M. Pierno, S. Descroix, J. L. Viovy, G. Mistura, Controlling the distance of highly confined droplets in a capillary by interfacial tension for merging on-demand, Lab Chip 19 (2019) 136–146, https://doi.org/10.1039/c8lc01182f.
[31] C.P. Lai, E.Y. Kim, C.E. Badr, R. Weissleder, T.R. Mempel, B.A. Tannous, X. O. Breakefield, Visualization and tracking of tumour extracellular vesicle delivery and RNA translation using multiplexed reporters, Nat. Commun. 6 (2015), https://doi.org/10.1038/ncomms8029.
[32] M.P. Zaborowski, K. Lee, Y.J. Na, A. Sammarco, X. Zhang, M. Iwanicki, P.S. Cheah, H.Y. Lin, M. Zinter, C.Y. Chou, G. Fulci, B.A. Tannous, C.P.K. Lai, M.J. Birrer, R. Weissleder, H. Lee, X.O. Breakefield, Methods for systematic identification of membrane proteins for specific capture of cancer-derived extracellular vesicles, Cell Rep. 27 (2019) 255–268.e6, https://doi.org/10.1016/j.celrep.2019.03.003.
[33] C.C. Damanti, E. Gaffo, F. Lovisa, A. Garbin, P. Di Battista, I. Gallingani, A. Tosato, M. Pillon, E. Carraro, M. Mascarin, C. Elia, A. Biffi, S. Bortoluzzi, L. Mussolin, MiR-26a-5p as a reference to normalize microrna QRT-PCR levels in plasma exosomes of pediatric hematological malignancies, Cells 10 (2021) 1–10, https://doi.org/10.3390/cells10010101.
[34] A.M. Nightingale, T.W. Phillips, J.H. Bannock, J.C. De Mello, Controlled multistep synthesis in a three-phase droplet reactor, 2014 51, Nat. Commun. 5 (2014) 1–8, https://doi.org/10.1038/ncomms4777.
[35] D. Ferraro, J. Champ, B. Teste, M. Serra, L. Malaquin, J.L. Viovy, P. De Cremoux, S. Descroix, Microfluidic platform combining droplets and magnetic tweezers: application to HER2 expression in cancer diagnosis, 2016 61, Sci. Rep. 6 (2016) 1–11, https://doi.org/10.1038/srep25540.
[36] T.D. Mai, D. Ferraro, N. Aboud, R. Renault, M. Serra, N.T. Tran, J.L. Viovy, C. Smadja, S. Descroix, M. Taverna, Single-step immunoassays and microfluidic droplet operation: Towards a versatile approach for detection of amyloid-β peptide-based biomarkers of Alzheimer's disease, Sens. Actuators, B Chem. 255 (2018) 2126–2135, https://doi.org/10.1016/j.snb.2017.09.003.
[37] M. Serra, D. Ferraro, I. Pereiro, J.L. Viovy, S. Descroix, The power of solid supports in multiphase and droplet-based microfluidics: towards clinical applications, Lab Chip 17 (2017) 3979–3999, https://doi.org/10.1039/C7LC00582B.
[38] M. Serra, T.D. Mai, A.L. Serra, M.C. Nguyen, A. Eisele, L. Perié, J.L. Viovy, D. Ferraro, S. Descroix, Integrated droplet microfluidic device for magnetic particles handling: Application to DNA size selection in NGS libraries preparation, Sens. Actuators B Chem. 305 (2020) 127346, https://doi.org/10.1016/J.SNB.2019.127346.
[39] F. Leccia, A. Nardone, S. Corvigno, L.Del Vecchio, S. De Placido, F. Salvatore, B. M. Veneziani, Cytometric and biochemical characterization of human breast cancer cells reveals heterogeneous myoepithelial phenotypes, Cytom. Part A. 81 A (2012) 960–972, https://doi.org/10.1002/cyto.a.22095.
[40] S.N. Hurwitz, M.A. Rider, J.L. Bundy, X. Liu, R.K. Singh, D.G. Meckes, Proteomic profiling of NCI-60 extracellular vesicles uncovers common protein cargo and cancer type-specific biomarkers, Oncotarget 7 (2016) 86999–87015, https://doi.org/10.18632/oncotarget.13569.
[41] M.I. Ramirez, M.G. Amorim, C. Gadelha, I. Milic, J.A. Welsh, V.M. Freitas, M. Nawaz, N. Akbar, Y. Couch, L. Makin, F. Cooke, A.L. Vettore, P.X. Batista, R. Freezor, J.A. Pezuk, L. Rosa-Fernandes, A.C.O. Carreira, A. Devitt, L. Jacobs, I. T. Silva, G. Coakley, D.N. Nunes, D. Carter, G. Palmisano, E. Dias-Neto, Technical challenges of working with extracellular vesicles, Nanoscale 10 (2018) 881–906, https://doi.org/10.1039/c7nr08360b.
[42] H.L. Cheng, C.Y. Fu, W.C. Kuo, Y.W. Chen, Y.S. Chen, Y.M. Lee, K.H. Li, C. Chen, H. P. Ma, P.C. Huang, Y.L. Wang, G. Bin Lee, Detecting miRNA biomarkers from extracellular vesicles for cardiovascular disease with a microfluidic system, Lab Chip 18 (2018) 2917–2925, https://doi.org/10.1039/c8lc00386f.
[43] A. Morales-Kastresana, J.C. Jones, Flow cytometric analysis of extracellular vesicles, in: Exosomes Microvesicles Methods Mol. Biol, Humana Press, New York, 2017, pp. 215–225, https://doi.org/10.1007/978-1-4939-6728-5_16.
[44] M.W. Kim, S. Park, H. Lee, H. Gwak, K.A. Hyun, J.Y. Kim, H. Il Jung, S. Il Kim, Multi-miRNA panel of tumor-derived extracellular vesicles as promising diagnostic biomarkers of early-stage breast cancer, Cancer Sci. 112 (2021) 5078–5087, https://doi.org/10.1111/cas.15155.
[45] O. Baldasici, V. Pileczki, D. Cruceriu, L.I. Gavrilas, O. Tudoran, L. Balacescu, L. Vlase, O. Balacescu, Breast cancer-delivered exosomal miRNA as liquid biopsy biomarkers for metastasis prediction: a focus on translational research with clinical applicability, Int. J. Mol. Sci. 23 (2022), https://doi.org/10.3390/ijms23169371.
[46] S. Donati, S. Ciuffi, M.L. Brandi, Human circulating miRNAs real-time qRT-PCR-based analysis: An overview of endogenous reference genes used for data normalization, Int. J. Mol. Sci. 20 (2019) 1–19, https://doi.org/10.3390/ijms20184353.
[47] S.A. Bustin, V. Benes, J.A. Garson, J. Hellemans, J. Huggett, M. Kubista, R. Mueller, T. Nolan, M.W. Pfaffl, G.L. Shipley, J. Vandesompele, C.T. Wittwer, The MIQE guidelines: minimum information for publication of quantitative real-time PCR experiments, Clin. Chem. 55 (2009) 611–622, https://doi.org/10.1373/CLINCHEM.2008.112797.
[48] D.T. Grob, N. Wise, O. Oduwole, S. Sheard, Magnetic susceptibility characterisation of superparamagnetic microspheres, J. Magn. Magn. Mater. 452 (2018) 134–140, https://doi.org/10.1016/j.jmmm.2017.12.007.
[49] R. Reverberi, L. Reverberi, Factors affecting the antigen-antibody reaction, Blood Transfus. 5 (2007) 227–240, https://doi.org/10.2450/2007.0047-07.
[50] K. Zhang, Y. Yue, S. Wu, W. Liu, J. Shi, Z. Zhang, Rapid capture and nondestructive release of extracellular vesicles using aptamer-based magnetic isolation, ACS Sens. 4 (2019) 1245–1251, https://doi.org/10.1021/acssensors.9b00060.
[51] D. Brambilla, L. Sola, A.M. Ferretti, E. Chiodi, N. Zarovni, D. Fortunato, M. Criscuoli, V. Dolo, I. Giusti, V. Murdica, K. Kluszczyńska, L. Czernek, M. Düchler, R. Vago, M. Chiari, EV separation: release of Intact Extracellular Vesicles Immunocaptured on Magnetic Particles, Anal. Chem. 93 (2021) 5476–5483, https://doi.org/10.1021/acs.analchem.0c05194.
[52] W. Nakai, T. Yoshida, D. Diez, Y. Miyatake, T. Nishibu, N. Imawaka, K. Naruse, Y. Sadamura, R. Hanayama, A novel affinity-based method for the isolation of highly purified extracellular vesicles, Sci. Rep. 6 (2016) 1–11, https://doi.org/10.1038/srep33935.
[53] C.L. Shih, K.Y. Chong, S.C. Hsu, H.J. Chien, C.T. Ma, J.W.C. Chang, C.J. Yu, C. C. Chiou, Development of a magnetic bead-based method for the collection of circulating extracellular vesicles, N. Biotechnol. 33 (2016) 116–122, https://doi.org/10.1016/j.nbt.2015.09.003.

Davide Ferraro is Researcher at the Physics and Astronomy Department of the University of Padova. His main research interests are in droplet microfluidics, microfabrication with interdisciplinary applications ranging from the fundamental studies to biomedical applications, such as cell, nucleic acid and extracellular vesicles analysis.